

1 **Aromatic hydrocarbons provide new insight into carbonate concretion formation and the**
2 **impact of eogenesis on organic matter**

3 **Authors:**

4 Plet, C.^{1,2}, Grice, K.^{1*}, Scarlett, G. A.¹, Ruebsam, W.³, Holman, I. A.¹, Schwark, L.³

5 ¹ WA-OIGC, School of Earth and Planetary Sciences, Curtin University, Kent St, Bentley WA 6102,
6 Australia

7 ² CSIRO Mineral Resources, ARRC, 26 Dick Perry Avenue, Kensington WA 6151, Australia

8 ³Department of Organic and Isotope Geochemistry, Institute of Geoscience, Christian Albrecht
9 University, Kiel 24118, Germany

10 *corresponding author: K.grice@curtin.edu.au

11 **Keywords:** phytanyl toluene, phytanyl benzene, stable isotopes, GC×GC-ToF-MS, microbial
12 eogenesis, PAHs

13

14 **ABSTRACT**

15 Investigation of aromatic biomarkers extracted from carbonate concretions can contribute to
16 characterize the enhanced microbial activity that mediates carbonate concretion formation. This
17 microbial footprint can be further inferred from the stable isotopic values of carbonate ($\delta^{13}\text{C}$) and
18 pyrite ($\delta^{34}\text{S}$). Here, we used a combination of GC-MS and GC×GC-ToF-MS to compare the aromatic
19 fractions of two Toarcian carbonate concretions from the *H. falciferum ammonite zone* of the
20 Posidonia Shale (SW-Germany) and their host sediment. The results revealed that *n*-alkylated and
21 phytanyl arenes were enhanced in the concretions relative to the host sediment. These findings
22 support a very early diagenetic (eogenetic) microbial source for alkylated and phytanyl arenes
23 derived from the microbial ecosystem mediating concretion formation. In contrast, aromatic

24 compounds formed by thermal maturation (e.g. polycyclic aromatic hydrocarbons, aromatic
25 steroids, organic sulphur compounds) remained invariant in host rock and concretion samples.
26 When combined with bulk sediment and concretion properties, the aromatic compounds
27 composition indicates that eogenetic microbial activity upon concretion growth does not diminish
28 organic matter quality.

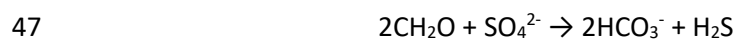
29 **1. INTRODUCTION**

30 Carbonate concretions are a common geological feature that is encountered in sedimentary rocks
31 throughout the geological record. They sometimes enclose exceptionally-preserved fossils (Grice et
32 al., 2019; Long and Trinajstic, 2010; Martill, 1989, 1988; Williams et al., 2015). Carbonate concretions
33 can also preserve information on the palaeoenvironment of deposition of their host sediments
34 (Grice et al., 2019; Plet et al., 2016). Concretions have been the focus of a large number of studies,
35 as highlighted in a review by Dietrich (2001)¹. Early on, Berner (1968, 1967) performed laboratory
36 experiments investigating the processes and timing involved in carbonate concretion. More recently,
37 Yoshida et al. (2018, 2015) succeeded in growing carbonate concretions around tusk shells in a
38 matter of weeks. In parallel to laboratory experiments, several studies have investigated the
39 geochemistry and petrology of carbonate concretions, indicating a pivotal role of microorganisms, in
40 particular, sulfate reducing bacteria and possibly archaea involved in the anaerobic oxidation of
41 methane (Coleman and Raiswell, 1995; Dale et al., 2014; Marshall and Pirrie, 2013; Martill, 1989).
42 The following microbially-mediated reactions are believed to play a crucial role in the formation of
43 the carbonate with the product of each of these reactions utilised by other microbial processes or
44 reacting with ions present in the immediate environment (Coleman, 1993; Coleman and Raiswell,
45 1995, 1980; Hendry et al., 2006; Lash and Blood, 2004):

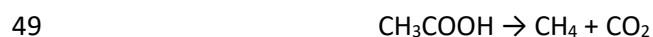
1

<https://web.archive.org/web/20081202111650/http://www.cst.cmich.edu/users/dietr1rv/concretions/index.htm>

46 Bacterial sulfate reduction (BSR)



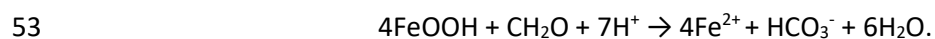
48 Methanogenesis



50 Anaerobic oxidation of methane



52 Bacterial iron reduction (FeR)



54 In particular settings, such as at methane seeps in the Black Sea, Reitner et al. (2005) investigated
55 the microbial mats surrounding carbonate concretions using molecular analyses (DNA). These
56 analyses evidenced the abundant sulfate reducing bacteria and archaea, in particular ANME-1
57 believed to be active players in the anaerobic oxidation of methane (AOM). Unfortunately,
58 accessible presently-forming carbonate concretions are rare (Boni et al., 1994; Coleman, 1993; Duan
59 et al., 1996; Pye et al., 1990), and most carbonate concretions investigated come from the
60 sedimentary record therefore challenging our understanding of microbial communities involved in
61 concretion formation. Although, the exact microbial communities involved in concretion formation
62 remain uncertain, models agree that carbonate concretions form around a centre of decaying
63 organic matter (OM) harbouring complex microbial communities within anoxic to euxinic sediments
64 (e.g. Coleman, 1993; Coleman and Raiswell, 1995).

65 Due to the labile nature of DNA molecules, DNA investigation of ancient carbonate concretions is
66 limited (Briggs and Summons, 2014). However, since lipids are more resilient to geological time and
67 processes, molecular studies of carbonate concretions can provide important insights into the
68 genetic processes leading to concretions (Briggs and Summons, 2014; Grice et al., 2019). Lipids were

69 first studied in carbonate concretions by Wolff et al. in 1992. This study highlighted the presence of
70 distinct lipid compositions for the different mineralogical zones of the concretion. In the dolomitic
71 zone, the presence of pentamethyleicosane (PMI) and squalane at trace levels were attributed to
72 the presence of methanogenic archaea. Since then, a range of molecular studies on lipids from
73 concretions has been conducted revealing the occurrence of several biomarkers attributed to
74 archaea and sulfate reducing bacteria, but also information on thermal maturity and
75 palaeoenvironments, for instance. An overview of these findings is presented in Table 1.

76 The investigations of lipids have largely focused on aliphatic hydrocarbons and fatty acids whereas
77 aromatic fractions of carbonate concretions have received much less attention (Table 1). Yet,
78 aromatic compounds can provide insightful information on the catagenetic kerogen maturation
79 state *via* investigation of PAHs or aromatic steroids but also about eogenetic and
80 palaeoenvironmental conditions. Carotenoids, for instance isorenieratene and its degradation
81 products - i.e. isorenieratane and aryl isoprenoids, are indicative of photic zone euxinic conditions
82 (e.g. Grice et al., 1996). Few studies investigated these compounds in carbonate concretions.
83 Melendez et al. (2013b) reported a range of carotenoids and aryl isoprenoids from a Devonian
84 concretion, the occurrence of isorenieratane and aryl isoprenoids were also reported from the
85 concretions investigated here (Plet et al., 2016). In the present study, we aim to gain further insights
86 into the processes and micro-ecosystems involved in concretion formation by comparing the
87 aromatic hydrocarbon distributions from concretions and host sediments using traditional GC-MS
88 and comprehensive two-dimensional gas chromatography time-of-flight mass spectrometry (GC×GC-
89 ToF-MS). This data was integrated with stable isotopic analyses of carbonate and sedimentary sulfur
90 ($\delta^{13}\text{C}$ of carbonate and $\delta^{34}\text{S}$ of mainly sulfide-bound S).

91

92 **2. GEOLOGICAL SETTING**

93 The Lower Toarcian (Early Jurassic; ~183 Ma) is marked by a global perturbation of the carbon cycle,
94 characterised by a negative carbon isotopic excursion related to release of ¹²C-enriched carbon to
95 the ocean-atmosphere system and global warming (e.g. Gómez et al., 2016; Hesselbo et al., 2000;
96 Kemp et al., 2005). These processes, which were potentially forced by changes in the Earth's solar
97 orbit (Bouilila and Hinnov, 2017; Kemp et al., 2005; Ruebsam et al., 2019), and were accompanied by
98 marine transgressions (Haq, 2018). These events resulted in the accumulation of OM-rich sediments
99 during a widespread oceanic anoxic event (OAE) in the Lower Toarcian. This OAE has been identified
100 in Europe, North America, South America, Asia, Australia and Madagascar (Jenkyns, 1988).

101 During the Lower Jurassic, Europe was located on an extensive shallow epicontinental shelf (West
102 Tethys shelf), which contained deeper sub-basins (Bassoulet et al., 1993; Röhl and Schmid-Röhl,
103 2005; Ziegler, 1990) . The SW Germany Basin, where the Posidonia Shale was deposited, is the focus
104 of a number of detailed organic geochemical studies (Schouten et al., 2000; Röhl et al., 2001;
105 Schmid-Röhl et al., 2002; Schwark and Frimmel, 2004). Deposition of early Lower Toarcian black
106 shales was linked to warm climates, a high sea level and prolonged water column stratification
107 (Frimmel et al., 2004; Hermoso et al., 2013; McArthur et al., 2008; Röhl et al., 2001). These
108 conditions promoted a shift of the chemocline from the sediment to water column, which in some
109 shelf areas led to the establishment of euxinic conditions (H₂S-rich waters) in the photic zone (photic
110 zone euxinia) (Ruebsam et al., 2018; Schouten et al., 2000; Schwark and Frimmel, 2004) .

111 **3. MATERIAL AND METHODS**

112 **3.1. Sampling location and preparation**

113 The concretions and the host sediment Posidonia Shale studied herein were collected from the
114 Holcim Cement quarry of Dotternhausen (SW-Germany) shortly after blasting. Although the exact
115 stratigraphic position remains unknown due to blasting, Plet et al. (2016) established that these
116 concretions derived from the lower *H. falciferum ammonite* zone, likely from above the Unterer
117 Stein carbonate horizon based on the comparison of microfacies, lithology and geochemical

118 signatures from the concretions with previous reports (Frimmel et al., 2004; Röhl et al., 2001;
119 Schwark and Frimmel, 2004). Both concretions have preserved a nucleus rich in OM (jet). The
120 concretion body is darker than the concretion rim and sedimentary bedding is preserved. Here, we
121 investigated sub-samples taken across bedding, however, the nuclei of the concretions were not
122 studied. Three samples were taken from each concretion. For both concretions, sample one was
123 taken from the inner concretion, sample two from the middle area of the concretion and sample
124 three was taken from the outer pyritic rim (Figure 1). These concretions were previously analysed
125 using microscopy and revealed micritic texture with dispersed small euhedral pyrite for sample one
126 and two, whereas sample three was characterised by abundant and larger pyrite crystals
127 agglomerated together (Plet et al., 2016).

128 **3.2. Whole rock geochemistry**

129 Elemental analyses of major and trace elements have been reported by Plet et al. (2016). Analyses
130 were performed using inductively coupled plasma mass spectrometry (ICP-MS) by ACTLABS
131 (Ancaster, Canada). Protocol information for the package Ultratrace 7 can be found on actlabs.com.
132 The carbonate concentration was inferred from the loss of weight during HCl treatment (HCl
133 concentration of 10% and 25%). Decalcified samples were analysed for their total organic carbon
134 content (TOC_{cf}) using a CNS-Elemental Analyzer (Elementar ®). The total organic carbon content of
135 the original sample (TOC) was then calculated by correcting the TOC_{cf} for carbonate concentration.
136 Earlier mineralogical and SEM-EDS investigations revealed that these concretions exclusively
137 contained calcite, pyrite and quartz (Plet et al., 2016). No other Fe-minerals commonly found in
138 concretions (e.g. ankerite, siderite) were detected. Therefore, the pyrite content was established
139 based on the assumption that the Fe is exclusively located in the pyrite of the concretions (Plet et al.,
140 2016). The Fe content, which was determined by ICP-MS, was used to calculate the pyrite content.
141 The Fe content was multiplied by 2.15 (stoichiometry of FeS₂). Finally, the residual input is
142 considered to correspond to the siliciclastic input.

143 **3.3. Stable isotope geochemistry**

144 3.3.1. $\delta^{13}\text{C}$ of carbonate

145 $\delta^{13}\text{C}$ values of carbonate in ground samples were determined with a Kiel III carbonate preparation
146 line connected to a Thermo Fisher 252 isotope ratio mass spectrometer (IRMS). The $\delta^{13}\text{C}$ values were
147 reported in per mil (‰) relative to Vienna PeeDee Belemnite (VPDB). Standard deviations were
148 <0.1‰.

149 3.3.2. $\delta^{34}\text{S}$ of bulk sediment

150 Stable sulfur isotopes ($\delta^{34}\text{S}$) were measured via combustion of the decalcified bulk-sample using a
151 Thermo EA elemental analyzer coupled to a Thermo Finnigan Delta V isotope ratio mass
152 spectrometer. Decalcification was achieved by HCl (10%) treatment and was carried out in order to
153 increase sulfur abundances. Afterwards, samples were washed, neutralized with deionized water
154 and dried in an oven at 40 °C (48 h). Sulfur isotope values were reported in conventional delta
155 notation relative to VCDT (Vienna Canyon Diablo Troilite). Reproducibility of the analysis is better
156 than 0.3‰. The $\delta^{34}\text{S}_{\text{bulk}}$ values reported here mainly reflect the isotopic composition of sulfide-bound
157 sulfur species, as the carbonate associated sulfur fraction was removed during HCl-treatment.

158 **3.4. Biomarkers**

159 To remove surficial organic contaminants, each sample block was washed in a mixture of
160 dichloromethane: methanol (DCM:MeOH) at 9:1 (v:v) for 15 mins in an ultrasonic bath. Samples
161 were then manually crushed, and ground in a zircon mill using benchtop ring mill (BRM, Rocklabs)
162 along with pre-annealed sand used as a procedural blank for lipid analyses. Procedures are reported
163 in more detail in Plet et al. (2016).

164 3.4.1. Soxhlet extraction

165 Each ground sample was Soxhlet extracted using a 9:1 mixture of DCM:MeOH for 72 h and activated
166 copper was added to remove elemental sulfur. Excess solvent was removed under a nitrogen purge

167 and concentrated total lipid extract (TLE) was adsorbed onto activated silica gel (160 °C, 24 h). TLE
168 was separated into aliphatic hydrocarbons eluted with *n*-hexane, aromatic hydrocarbons eluted with
169 a mixture of *n*-hexane:DCM (7:3) and polar compounds eluted with DCM:MeOH (1:1) using a large
170 column (20 cm x 0.9 cm i.d.).

171 3.4.2. Gas chromatography mass spectrometry (GC-MS) analyses

172 Aromatic fractions were analysed on an Agilent 6890 gas chromatographs (GC) interfaced with an
173 Agilent 5973 mass selective detector (MSD). The GC was equipped with a DB-5MS column [60 m ×
174 0.25 mm coated with a 0.25 µm film thickness] and a split/splitless injector operated in splitless
175 mode. The oven temperature was programmed from 40 °C to 325 °C (3 °C min⁻¹), with initial and
176 final temperature hold for 1 min and 30 min, respectively. Ultra-high purity helium was used as a
177 carrier gas at a constant flow of 1.1 mL min⁻¹. Electron ionisation mass spectra were acquired in full
178 scan mode at 4 scans s⁻¹ and at 70 eV electron energy.

179 3.4.3. GCxGC-ToF-MS

180 Aromatic fractions were analysed using a Leco Pegasus IV system equipped with dual stage cryogenic
181 modulator (Leco, Saint Joseph, MI, USA). The primary column was a 60 m × 0.25 mm × 0.25 µm DB
182 5MS (Agilent, Santa Clara, CA, USA) coupled to a secondary 1.2 m × 0.15 mm × 0.15 µm BPX50 (SGE
183 Analytical Science Pty Ltd, Ringwood, Victoria, Australia). The carrier gas was ultrahigh purity helium
184 with constant flow of 1.5 mL min⁻¹. The inlet temperature was 310 °C with 1 µL injection. Conditions
185 were: 50 °C (1 min isothermal), then 2.5 °C min⁻¹ to 310 °C, (isothermal 15 min) and a modulation
186 period of 3 s, with secondary oven offset of 10 °C and modulator offset of 15 °C. The mass
187 spectrometer was operated at 70 eV electron energy; the ion source temperature was 250 °C and
188 the transfer line 315 °C. The scan speed was 100 Hz with a range of 45–600 Daltons (Da). ChromaTOF
189 (LECO) software package was used for instrument control and data analysis. Minimum acceptable
190 signal to noise ratio was 30:1.

191

192 3.4.4. Gas chromatography isotope ratio mass spectrometry (GC-irMS) analyses

193 Compound specific stable isotope analyses were performed using a Thermo Delta Advantage isotope
194 ratio mass spectrometer couple to a Thermo Trace GC Ultra via a GC Isolink and Conflo IV. GC
195 conditions were similar to the ones previously described for the GC MS analyses. The $\delta^{13}\text{C}$ values
196 were determined by integration of the masses 44, 45 and 46 using Thermo Isodat software and
197 manually evaluated. Comparison of the samples to a mixture of *n*-alkanes with known $\delta^{13}\text{C}$ values
198 was used to calibrate the values to the VPDB scale. Samples were run in duplicate.

199 **4. RESULTS**

200 **4.1. Aromatic hydrocarbons**

201 4.1.1. Evaluation of the resilience of aromatic hydrocarbon compounds

202 All aromatic fractions were highly similar in their overall molecular composition (Figure 2). However,
203 the unresolved complex mixture (UCM) was relatively enhanced in the concretions compared to the
204 host sediment suggesting a slightly higher degree of biodegradation in the concretions (Trolio et al.,
205 1999). In addition, Plet et al. (2016) reported that the host sediment presents the highest hydrogen
206 index (HI) values (820 mgHC/gTOC), whereas the concretion samples revealed lower values (580 to
207 740 mgH/gTOC). In the present samples, which have a low maturity ($R_0 \sim 0.5\%$, Frimmel et al., 2004),
208 the concretion samples show lower HI compared to the host sediment. The HI indicates a higher
209 degree of kerogen preservation in the host sediment than in the concretions .

210 Three compound classes were assessed for their resilience towards thermal maturation and
211 biodegradation: i) methyltrimethyltridecylchromans (MTTCs); ii) methylated phenanthrenes and
212 dibenzothiophenes (MP and MDBT, respectively) and iii) triaromatic steroids (TAS) (Figure 3). To
213 identify the most resilient compound group, we determined the degree of OM preservation using HI
214 values reported in Plet et al. (2016) and compared the relative evolution of the three compound

215 groups. We assumed that the most resilient compounds of the three groups would present a relative
216 increase in the samples demonstrating the lowest HI values (Table 2) – i.e. concretion rim samples
217 A3 and B3. Both MTTCs and TAS relatively increased in samples A3 and B3 (Figure 3). However, the
218 relative increase of TAS was higher (~10 %) than that of MTTC (~5 %) from the sample presenting the
219 greater HI –i.e. host sediment, and samples with the lower HI –i.e. concretion rims (A3 and B3).
220 Therefore, all compounds presented here were normalised to TAS.

221 4.1.5. PAHs and organic sulphur compounds

222 Polycyclic aromatic hydrocarbons (PAHs) are relatively low in abundance in all samples (Figure 2).
223 The aromatic hydrocarbon distribution is characterised by abundant methyl dibenzothiophenes
224 (MDBTs), mono-, di- and tri-MTTCs and aromatic steroids. In addition to these compounds, two large
225 peaks I and II were identified as 1,1,7,8-tetramethyl-1,2,3,4-tetrahydrophenanthrene (Azevedo et
226 al., 1992; Sinnighe Damsté et al., 1999) and C₃ alkylphenanthrene (Killops, 1991), respectively.
227 Phenanthrene and mono- to tetra-methylated analogues as well as methylated naphthalene
228 homologues were detected in all samples. However, larger unsubstituted ≥4rings PAHs are either
229 present as trace (e.g. benzo[ghi]perylene) or were found to be below detection limits. Sulphur
230 compounds, such as dibenzothiophene (DBT) as well as methyl- (MDBTs) and dimethyl- (DMDBTs)
231 substituted homologues are abundant in all samples, whereas trimethyl-DBTs (TMDBTs) were only
232 present in traces. Three benzonaphthothiophene (BNT) isomers were also present. The relative
233 distribution of the sulphur-bearing compounds shows some strong similarities between the different
234 samples. Methyl-substituted 1-MDBT is particularly abundant and constitutes one of the major
235 peaks of the total ion chromatograms (Figure 1). The normalisation of aromatic compounds or
236 compound classes to TAS suggests that DBT, MDBTs and DMDBTs compounds are relatively more
237 abundant in the host sediment and the innermost concretion body samples and are less abundant in
238 the concretion rims with exception of sample A2.

239 4.1.2. Alkylated and phytanyl arenes

240 Alkylated and phytanyl benzene and toluene were identified in all concretion samples using
241 traditional GC-MS analyses (Ostroukhov et al., 1983). Extracted ion chromatograms (m/z 92) of the
242 host sediment presented several minor peaks showing some degree of co-elution and no alkylated
243 benzene nor phytanyl benzene were identified (Figure 4). The low intensity coupled with some
244 coelution of these minor peaks prevented from comparison and challenged the interpretation.
245 Therefore, we used GC×GC-ToF-MS to overcome this issue by avoiding co-elution in the polar
246 dimension. For identification and relative quantification purposes, alkylated and phytanyl benzenes
247 were extracted using m/z 91 and m/z 92 whereas alkylated and phytanyltoluenes were measured on
248 m/z 105 and m/z 106. The GC×GC-ToF-MS analyses revealed that alkylbenzenes and
249 phytanylbenzene were also present in the host sediment. The distribution of alkylated benzenes was
250 similar in all samples, maximizing at C_{18} and C_{20} and decreasing to trace level for compounds $>C_{28}$. To
251 compare the relative abundances of the alkylated benzenes and alkylated toluenes across the
252 different samples, we define the AlBr (alkylbenzene ratio= $\text{sum alkyl benzenes}/\text{sum } C_{26}\text{-}C_{28}$ TAS) and
253 the AlTr (alkyltoluene ratio= $\text{sum alkyltoluenes}/\text{sum } C_{26}\text{-}C_{28}$ TAS) ratios. The AlBr is 10 times greater in
254 both concretion samples than in the host sediment (Table 3). Phytanylbenzene is also present in
255 relatively low abundances in concretion samples (Table 3). The alkylated toluenes were detected in
256 all samples (Figure 4) and the newly defined AlTr ratio is 4 to 11 times greater in the concretion
257 samples than in the host sediment. Phytanyl toluene is also more abundant in the concretion
258 samples (Table 3) than in the host sediment. The ratio of phytanyl toluene to TAS is 3.5 to 13 times
259 greater in the concretion than in the host sediment (Table 3). In the two rim samples, A3 and B3,
260 $\delta^{13}\text{C}$ values of phytanyl toluene were measured. Sample A3 ($\delta^{13}\text{C} = -36.1 \text{‰} \pm 0.5$) is slightly less ^{13}C -
261 depleted than sample B3 ($\delta^{13}\text{C} = -38.1 \text{‰} \pm 0.4$).

262 In addition, the GC×GC-ToF-MS analyses showed the presence of a range of toluene compounds with
263 isoprenoid branching (supplementary Figure 1). These branched toluenes (C_{16} BrT, C_{18} BrT, C_{23} BrT,
264 C_{26} BrT) were identified in all samples (m/z 106), sometimes at trace levels only. To compare their
265 relative abundances across the sample set, the following ratio was defined: BrTr= $\text{sum } C_{16}\text{-}C_{26}$ BrT *

266 1000 / sum C₂₆-C₂₈ TAS. The BrTr shows that these compounds are relatively less abundant in the
267 host sediment than in concretion samples, by as much as 20 times in sample B1 and as little as three
268 times in sample A2 (Table 3).

269 4.1.3. Alkylated naphthalenes

270 Alkylated naphthalenes are present in all samples with side chain lengths comprised between C₃ and
271 C₂₁, although only concretion samples (A1, A3 and B1) contain long alkylated homologues (side chain
272 > C₁₅). All samples are maximizing at C₁₇-C₁₈ (alkylated naphthalenes with a side chain of C₇-C₈). The
273 ratios of alkylated naphthalene to TAS (sum AlkN /sum C₂₆-C₂₈ TAS) highlight that alkylated
274 naphthalenes are slightly more abundant in the concretion than in the host sediment (Table 3).

275 4.1.6. Aromatic hopanoids

276 The identification of aromatic hopanoids was performed based on comparison with published data
277 [mass spectra and retention order; (Hussler et al., 1984; Killops, 1991)]. Although the GC-MS
278 analyses suggested most aromatic secohopanoid compounds reported in Killops (1991) were present
279 in the concretion samples, GC×GC-ToF-MS analyses revealed that most of these compounds are co-
280 eluting in the polar dimension with other compounds. C₂₉-D,E-aromatised-8,14-secohopanoid
281 (Supplementary Figure 2) and C₂₉-C₃₀ D-ring aromatised 8,14-secohopanoids were present
282 (Supplementary Figure 3). In addition, benzohopanes (C₃₁ – C₃₅) were also detected in all samples
283 both by GC-MS and GC×GC-ToF-MS. C₃₂ and C₃₃ benzohopanes were the most abundant throughout
284 the sample set and were integrated from the TIC using GC×GC-ToF-MS. To compare the relative
285 abundances of these compounds across samples, the peak area normalisation of C₂₉ D,E-ring
286 aromatised 8,14-secohopane (C₂₉DESHr) and C₃₂-C₃₃ benzohopane (BHR) to TAS was performed on
287 GC×GC-ToF-MS data (Table 3). These ratios revealed i) more abundant C₂₉-D,E-ring aromatised 8,14-
288 secohopanoid in the concretion than in the host sediment; ii) greater benzohopane content in the
289 host sediment than in the concretion, iii) within the concretions, the benzohopane relative
290 abundance increased towards the rim.

291 4.1.7. Aryl isoprenoids and MTTC

292 The identification of aryl isoprenoids within these concretions was previously reported in (Plet et al.,
293 2016). In brief, isorenieratane and aryl isoprenoids with a 2,3,6-substitution pattern are present in
294 the host sediment, but were only detected in trace abundance in the carbonate concretions and the
295 aryl isoprenoid ratio was consistent with persistent reductive environmental conditions (Schwark
296 and Frimmel, 2004). MTTC are relatively abundant in all samples. MTTC ratio as defined by Sinninghe
297 Damsté et al. (1993, 1988b) are remarkably constant for all samples ($=0.63\pm 0.01$).

298 **4.2. Whole rock geochemistry and stable isotope analyses**

299 High proportion of carbonate cements in carbonate concretions (>70 %) can easily overprint the
300 original signal inherited from the host sediment. This process, commonly referred to as carbonate
301 dilution, can lead to the host sediment signature being too low to be detected. For instance, this
302 carbonate dilution can explain why detrital components were not detected by powder XRD analyses
303 reported in Plet et al. (2016), although quartz grains were observed using SEM analyses..

304 The variations in mineral abundances between the host sediment and the two carbonate
305 concretions (bodies and rims) are presented in Table 2. In the host sediment, the siliciclastic and
306 carbonate component are of similar relative abundance (~40 wt%, Table 2), and the pyrite and TOC
307 proportions are also similar (~ 10 wt%). In contrast, all concretions samples are clearly dominated by
308 carbonate: >95 wt% for the concretion body and >75 % for the concretion rim. The rim is also
309 characterised by a greater pyrite component ~17.5 wt% in average than the concretion body (1 wt%)
310 and the host sediment (7 wt%).

311 Pyrite is more ^{34}S -enriched in the concretion than in the host sediment (table 2). Moreover, the
312 $\delta^{34}\text{S}_{\text{bulk}}$ and $\delta^{13}\text{C}_{\text{carbonate}}$ values in the concretions co-vary, displaying more negative values in the
313 concretion body than in the concretion rim (Table 2).

314 **5. DISCUSSION**

315 **5.1. Distribution of catagenetic aromatic hydrocarbons and microbial eogenesis: significance**
316 **for kerogen quality**

317 The HI indicates a better preservation of the organic matter in the host sediment compared to the
318 concretion. This may appear contradictory given that carbonate concretions are known for their
319 exceptional preservation of organic matter and fossils. Here, we attribute the low HI in concretion
320 samples to the microbial eogenetic activity rather than burial diagenesis. We suggest that in a
321 context of more mature settings such as the ones reported by Dong et al. (2008), the concretion
322 actually protects the organic matter from further degradation related to burial diagenesis and
323 catagenetic processes.

324 The majority of PAHs and aromatic steroids commonly form during late diagenesis, i.e. catagenetic
325 processes, such as the cracking of sedimentary OM during sediment burial, which occurs at basin
326 scale. In contrast, processes related to microbial eogenesis that occur during the very early stages of
327 diagenesis can be highly localised. Microbial eogenesis includes the mineralisation of OM by
328 microbial processes (e.g. sulfate reduction, iron reduction, methanogenesis and methanotrophy),
329 which would decrease HI values, and can induce the precipitation of carbonate cement (e.g. Riding,
330 2000) as well as pyrite framboids (e.g. Wilkin and Barnes, 1997). In the present study, the concretion
331 samples are characterised by high CaCO₃ content (up to 97 wt%, Table 2) with their overall
332 carbonate content being twice as abundant as that of the host sediment (Table 2). During microbial
333 degradation of the OM, organic carbon is mineralised into HCO₃⁻ which is, in turn, assimilated into
334 the formation of CaCO₃ present in the concretion..

335 Yet, diagenetic compounds, commonly ≤4 ring PAHs such as naphthalenes, phenanthrene and
336 homologues, DBT and methyl-substituted homologues, were detected in both the concretion and
337 host shale samples. In addition, the overall distribution of aromatic steroids is similar for all samples;
338 although the rim samples display a relative increase of triaromatic steroids compared to other
339 aromatic compounds (Figure 3). The similarities in catagenetic compound distributions indicate that

340 the kerogen from which they derive was similar in both the concretions and in the host sediment,
341 despite of the microbial metabolization of OM during carbonate concretion growth. Eogenetic
342 concretion growth thus has not altered the kerogen's potential for generation of aromatic
343 hydrocarbons. These observations are in agreement with previous studies of biomarkers in
344 carbonate concretions (Boni et al., 1994; Marynowski et al., 2007; Zatoń and Marynowski, 2004) and
345 suggest that although the quantity of OM is affected by microbial metabolism involved in concretion
346 growth, the petroleum formation potential of the OM has not suffered from these eogenetic
347 processes. Formation of carbonate concretions in petroleum source rocks thus does not diminish
348 their oil generation capacities.

349

350 5.2. Inferred microbial activity in the concretion from the variations of $\delta^{13}\text{C}_{\text{carbonate}}$ and $\delta^{34}\text{S}_{\text{bulk}}$

351 Stable carbon isotopic values are of importance to refine microbial processes in concretion genesis.
352 In the present study, the stable carbon isotopic signatures of carbonate from the concretion samples
353 are more ^{13}C -depleted than in the host sediment (^{13}C values from -17 ‰ to -8.3 ‰ in the concretions
354 *versus* -1.8 ‰ in the host sediment). The $\delta^{13}\text{C}$ values, measured in the concretions, are in line with
355 previous reports of Jurassic calcite concretions presenting a pyrite rim (e.g. Coleman and Raiswell,
356 1995, 1980). These studies attributed the ^{13}C -depletion of the carbonate from the concretion to the
357 enhanced activity of sulfate reducing bacteria.

358 In addition, in anoxic sedimentary environment enhanced bacterial sulfate reduction may also be
359 recorded in the sulfur stable isotopic composition of sedimentary pyrite (Berner et al., 2013;
360 Borowski et al., 2013; Lin et al., 2016). In this study, $\delta^{34}\text{S}_{\text{bulk}}$ values are more positive in the
361 concretion than in the host sediment (Table 2). However, $\delta^{34}\text{S}_{\text{bulk}}$ value of the host sediment is more
362 positive than common values from marine environments (Werne et al., 2003; Wilkin and Arthur,
363 2001). According to Berner et al. (2013), such $\delta^{34}\text{S}_{\text{pyrite}}$ values for marine sediments could be related

364 to the accumulation of sedimentary pyrite under sulfate limitation within the SW-German sub-basin,
365 which had restricted connection to the open ocean.

366 Variations in stable isotopic composition were also measured within a single concretion. Although
367 the values were not identical for both concretions, a similar trend was observed. Concretion A and
368 concretion B revealed an increase in $\delta^{13}\text{C}_{\text{carbonate}}$ and $\delta^{34}\text{S}_{\text{bulk}}$ values in the rim (Table 2). This increase
369 coincides with a rise in pyrite content (from ~1 wt% up to ~ 22 wt % in concretion B). Such variations
370 in Jurassic pyritiferous carbonate concretions were previously reported in association with a change
371 from framboidal pyrite, in the concretion body, to euhedral pyrite in the concretion rim. They were
372 also attributed to either a temporal or spatial control on concretion growth, with a strong
373 contribution of sulfate reducing bacteria to the carbonate and sulfide pool (Coleman, 1993; Coleman
374 and Raiswell, 1995).

375 Here, the concretion contained dominantly euhedral pyrite in both concretion body and rim (Plet et
376 al., 2016), which suggest a high rate of microbial sulfate reduction generating sulfide more rapidly
377 than the iron was supplied to the system from external sources (Coleman and Raiswell, 1995). In the
378 present samples, the preservation of an OM-rich nucleus also indicates a rapid isolation from the
379 surrounding environment, either by the precipitation of a carbonate cement (Martill, 1989), the
380 formation of Ca soap (Berner, 1968; Thiel and Hoppert, 2018), or the entombment within a microbial
381 mat (Reitner et al., 2005).

382 In this closed system, we hypothesise that the degradation of OM by microbial sulfate reduction was
383 such that microbes consumed all light ^{12}C and ^{32}S isotope available and therefore, had to rely on the
384 heavier isotope (^{13}C and ^{34}S) to sustain their activity. This would have resulted in an increasingly
385 heavier carbon and sulfide pool through time. This hypothesis suggests that the heavier stable
386 isotopic composition of the concretion rim reflects an outward concretion growth, i.e. formation of
387 the mineral in the concretion body followed by the concretion rim.

388 An alternative explanation, however, could be a simultaneous formation of concretion body and rim
389 with distinct dominant microbial communities forming each of them. The carbonate cement with the
390 greatest ¹³C-depletion along with lowest pyrite content observed in the concretion body could
391 indicate a greater contribution of anaerobic methane oxidisers (archaea), whereas a greater pyrite
392 content along with more ³⁴S-enriched pyrite in the rim would point to greater input from bacterial
393 sulfate reduction. Generally, studies of calcium carbonate concretions attribute most of the
394 carbonate production to microbial sulfate reduction, although the activity of micro-organisms
395 involved in the methane cycle – i.e. methanogenesis and anaerobic oxidation of methane – is also
396 mentioned (Coleman and Raiswell, 1995; Curtis et al., 1987; Duan et al., 1996; Huggett, 1994;
397 Raiswell and Fisher, 2000; Scotchman, 1991). Concretionary carbonate presently forming at
398 methane seeps in the Black Sea revealed the presence of microbial mats able to perform both
399 sulfate reduction and anaerobic oxidation of methane (Reitner et al., 2005). Although methane
400 seeps are not a prerequisite for the formation of carbonate concretions, the study by Reitner et al.
401 (2005) revealed how organisms involved in methanogenesis and anaerobic oxidation of methane are
402 both actively contributing to the microbial ecosystem leading to concretion formation, along with
403 sulfate-reducing bacteria.

404 Both a temporal decrease in light stable isotopes available (Rayleigh distillation) and a spatial change
405 in the microbial ecosystem could result in the pyrite content as well as the stable isotopic variations
406 observed, and these hypotheses are not necessarily exclusive. Although the exact mechanisms of
407 carbonate concretion formation remain to be fully understood, evidence of exceptional preservation
408 of fossils (e.g. Martill, 1989, 1988; Plet et al., 2017; Williams et al., 2015) and biomolecules
409 (Melendez et al., 2013a; Plet et al., 2017) indicate a system rapidly isolated from the surrounding
410 environment. This is also confirmed by laboratory experiments (Berner, 1968, 1967; Yoshida et al.,
411 2018, 2015) and dating studies (Yoshida et al., 2019).

412 5.3. Alkylated and phytanyl arenes distribution and significance

413 An additional aspect of this study relates to the alkylated and phytanyl arenes (supplementary Figure
414 4). Alkylated benzenes are common laboratory contaminants due to their use in detergents. In order
415 to be confident that all the monoaromatic compounds identified in the samples were not artefacts
416 resulting from the work-up procedures, repeated extractions were performed using multiple
417 procedural blanks. When analysed by GC-MS and GCxGC-TOFMS, none of the blanks contained any
418 of compounds reported herein and are therefore authentic biomarkers of the concretions.

419 These compounds, particularly phytanyltoluene, show high relative abundance in the concretion
420 samples in comparison to the host sediment. Such an elevated relative abundance indicates that the
421 source organisms of these compounds thrive in concretion-forming ecosystems. Although alkylated
422 and phytanyl arenes have been widely reported in sedimentary OM and oils (e.g. Grotheer et al.,
423 2017; Sinninghe Damsté et al., 1993, 1988b; Williams et al., 1988; Zhang et al., 2014), their origin
424 presently remains unclear (Grotheer et al., 2017 and references therein). Amongst the different
425 hypotheses proposed, the direct biosynthesis by hypersaline archaeal communities (Sinninghe
426 Damsté et al., 1993, 1988b) is of interest here. As discussed above, it has been suggested that
427 archaea could be major contributors to concretion-forming microbial ecosystems (De Boever et al.,
428 2009; Hendry et al., 2006; Lash and Blood, 2004; Reitner et al., 2005; Wolff et al., 1992; Woo and
429 Khim, 2006). In order to further test this hypothesis in the present context and determine the degree
430 of salinity during concretion formation, the MTTC ratio was calculated (Sinninghe Damsté et al.,
431 1993, 1988a). This ratio provides insight into palaeosalinity with low values (<0.4) reflecting
432 hypersaline conditions (Sinninghe Damsté et al., 1987, 1988a, 1993; Grice et al., 1998; Tulipani et al.,
433 2015). Here, the MTTC ratio is not representative of hypersaline conditions and is remarkably
434 constant for all samples ($=0.63 \pm 0.01$). This value for the MTTC ratio coincides with normal marine
435 conditions at the time of concretion formation. Our results therefore do not indicate that alkylated
436 and phytanyl arenes originate from halophilic archaea. These observations are supported by a
437 previous study on the Permian-Triassic Boundary (~252 Ma) which also reported abundant phytanyl
438 arenes despite an absence of paleo-hypersaline conditions (Grotheer et al., 2017).

439 Stable carbon isotopic composition of phytanyltoluene can be used to further determine the origin
440 of this compound. In the rim samples, $\delta^{13}\text{C}_{\text{PT}}$ values are up to 3.4 ‰ more negative than previously
441 reported values of *n*-alkanes from the same concretions (Plet et al., 2016). Interestingly, an inverse
442 trend is usually observed for aromatic compounds: aromatics are commonly more ^{13}C -enriched than
443 *n*-alkanes from a similar sediment or oil sample (Holman and Grice, 2018).

444 Here, the $\delta^{13}\text{C}_{\text{PT}}$ values, -36.1 ‰ and -38.1 ‰ for concretion A and concretion B, respectively, are
445 more ^{13}C -enriched than common biomarkers of archaea involved in methane cycling (e.g. Hinrichs
446 and Boetius, 2002). Moreover, no additional archaeal biomarker was detected in any of the samples.
447 The greater relative abundance of alkylated and phytanyl arenes, along with the C_{29} D,E-ring
448 diaromatic secohopanoid, a potential bacterial marker, in the concretion suggests that phytanyl and
449 *n*-alkylated arenes probably derive from a type of bacteria particularly active in the microbial
450 ecosystem leading to concretion formation. Benzohopanoids also increase in the rim compared to
451 the concretion body, however they are relatively more abundant in the host sediment. This
452 benzohopane distribution suggests a different bacterial source that is not particularly abundant in
453 the micro-ecosystem of the concretion.

454 To better constrain the origin of the alkylated and phytanyl arenes in carbonate concretion,
455 correlation coefficients were calculated. The correlations coefficients were determined both
456 including and excluding the host sediment sample to highlight the differences and the likely origin of
457 the *n*-alkylated and phytanyl arenes compounds (Figure 5). PTr and PBr showed a high correlation
458 coefficient (Figure 5A) when the host sediment was included ($r^2=0.9$ ($n=7$)). However, a slightly higher
459 correlation was achieved when the host sediment sample was excluded ($r^2=0.93$, $n=6$). This strong
460 correlation, although on a small dataset, supports a common source for these compounds in the
461 concretions. Grotheer et al. (2017) detected phytanylbenzene and phytanyltoluene along with C_{33} *n*-
462 alkyl cyclohexane (C_{33} *n*-ACH) compounds in black shale samples from the Permian-Triassic
463 Boundary. The authors reported a very strong correlation ($r^2=0.99$) between phytanylbenzene and

464 phytanyltoluene, indicating a common source for these compounds in samples from high latitude
465 environments. However, the compounds were not detected in samples from carbonate-rich low
466 latitude environments (Grotheer et al., 2017). Here, no C₃₃ *n*-ACH was detected, supporting this
467 biomarker is characteristic of samples from the Permian-Triassic crisis (Grice et al., 2005). In
468 addition, the concretions were formed in warm, mid-latitude climate (Gómez et al., 2016; Rodrigues
469 et al., 2019) , indicating that the source organism is not exclusive to cooler environment but thrives
470 in concretion-forming microbial ecosystem. Correlation coefficients between AlkBr and AlkTr, AlkBr
471 and PBr, and AlkTr and PTr (all with $r^2 < 0.9$, $n=7$, Figure 5B-D) are lower than for phytanyl compounds
472 ($r^2 > 0.9$; Figure 5A) and decrease when the host sediment sample is excluded from the dataset. In
473 particular, the correlation coefficients of AlkBr/PBr and AlkTr/PTr (r^2 values of 0.66 and 0.37,
474 respectively) in the carbonate concretion highlight a different source for alkylated *versus* phytanyl
475 compounds.

476 **6. CONCLUSIONS**

477 The detailed examination of the aromatic fractions from carbonate concretions and their host
478 sediment highlights microbial processes involved in carbonate concretion formation. In addition to
479 bulk stable isotopes supporting enhanced and complex microbial activity, the present study
480 demonstrates that:

- 481 • Stable isotopic values of calcite and sedimentary sulfur (mainly pyrite) ($\delta^{13}\text{C}$ and $\delta^{34}\text{S}$,
482 respectively) co-vary. The ^{13}C -depleted carbonate cement from the concretion body results
483 from microbial activity relying on a ^{13}C -depleted source.
- 484 • The increase in $\delta^{34}\text{S}$ values in the rim associated with greater pyrite content indicates that
485 microbial sulfate reduction under successively higher ^{32}S -depletion of the sulfate pool is
486 largely responsible for pyritic rim genesis.
- 487 • Phytanylbenzene and phytanyltoluene share a similar biological source, thriving in
488 concretion-forming microbial ecosystem.

489 • *n*-alkylated and phytanyl arenes do not share a common source in concretion-forming
490 ecosystem. Although a clear origin for these compounds was not identified, it is likely that, in
491 this specific setting, halophilic archaea were not the source organisms.

492 Our study of two Toarcian carbonate concretions along with their host sediment indicates that *n*-
493 alkylated and phytanylbenzenes and toluenes could provide some insight into the processes of
494 carbonate concretion formations. Constraining the source of these compounds could improve our
495 understanding of ancient microbial ecosystems forming these concretions. Furthermore, it would
496 provide clues to unravel how the kerogen quality remained unaffected by the enhanced microbial
497 activity during carbonate concretion formation.

498

499 **ACKNOWLEDGMENTS**

500 This research was supported by a Discovery Grant from the Australian Research Council (ARC-DORA-
501 Kliti Grice, DP130100577) and DFG grants Schw554/23 and Schw554/29. Peter Hoper is thanked for
502 GC-MS technical support. Marieke Sieverding is thanked for $\delta^{34}\text{S}$ technical support. CP thanks Curtin
503 University and The Institute of Geoscience Research for a PhD and a Top-up scholarship. The authors
504 wish to acknowledge Anais Pages for constructive criticisms that contributed to the improvement of
505 an earlier version of this paper. We thank two anonymous reviewers for their constructive
506 comments.

507 **REFERENCES**

508 Azevedo, D.A., Aquino Neto, F.R., Simoneit, B.R.T., Pinto, A.C., 1992. Novel series of tricyclic aromatic
509 terpanes characterized in Tasmanian tasmanite. *Org. Geochem.* 18, 9–16.

510 [https://doi.org/10.1016/0146-6380\(92\)90138-N](https://doi.org/10.1016/0146-6380(92)90138-N)

511 Bassoulet, J.P., Elmi, S., A.P., Cecca, F., Bellion, Y., Guiraud, R., Baudin, F., 1993. Mid-Toarcian, in:

512 Dercourt, J., Ricou, L.E., Vrielynck, B. (Eds.), *Atlas Tethys Paleoenvironmental Maps*. BEICIP —

513 FRANLAB, Rueil-Malmaison, pp. 63–84.

514 Baumann, L.M.F., Birgel, D., Wagreich, M., Peckmann, J., 2016. Microbially-driven formation of
515 Cenozoic siderite and calcite concretions from eastern Austria. *Austrian J. Earth Sci.* 109.
516 <https://doi.org/10.17738/ajes.2016.0016>

517 Berner, R.A., 1968. Calcium carbonate concretions formed by the decomposition of organic matter.
518 *Science* (80-.). 159, 195–197.

519 Berner, R.A., 1967. Rate of concretion growth. *Geochim. Cosmochim. Acta* 32, 477–483.

520 Berner, Z.A., Puchelt, H., Nöltner, T., Kramar, U., 2013. Pyrite geochemistry in the Toarcian Posidonia
521 Shale of south-west Germany: Evidence for contrasting trace-element patterns of diagenetic
522 and syngenetic pyrites. *Sedimentology* 60, 548–573. [https://doi.org/10.1111/j.1365-](https://doi.org/10.1111/j.1365-3091.2012.01350.x)
523 [3091.2012.01350.x](https://doi.org/10.1111/j.1365-3091.2012.01350.x)

524 Boni, M., Simoneit, B.R.T., Leif, R.N., Mckenzie, J.A., 1994. 15 . Organic Matter and Carbon Isotope
525 Composition of Carbonate Nodules and Associated Sediments From Middle Valley , Leg 139 1.
526 *Proc. Ocean Drill. Program, Sci. Results* 139.

527 Borowski, W.S., Rodriguez, N.M., Paull, C.K., Ussler, W., 2013. Are 34S-enriched authigenic sulfide
528 minerals a proxy for elevated methane flux and gas hydrates in the geologic record? *Mar. Pet.*
529 *Geol.* 43, 381–395. <https://doi.org/10.1016/j.marpetgeo.2012.12.009>

530 Boulila, S., Hinnov, L., 2017. A review of tempo and scale of the early Jurassic Toarcian OAE:
531 implications for carbon cycle and sea level variations. *Newsletters Stratigr.* 50, 363–389.

532 Briggs, D.E.G., Summons, R.E., 2014. Ancient biomolecules: their origins, fossilization, and role in
533 revealing the history of life. *Bioessays* 36, 482–90. <https://doi.org/10.1002/bies.201400010>

534 Coleman, M.L., 1993. Microbial processes: Controls on the shape and composition of carbonate
535 concretions. *Mar. Geol.* 113, 127–140. [https://doi.org/10.1016/0025-3227\(93\)90154-N](https://doi.org/10.1016/0025-3227(93)90154-N)

536 Coleman, M.L., Raiswell, R., 1995. Source of carbonate and origin of zonation in pyritiferous
537 carbonate concretions: evaluation of a dynamic model. *Am. J. Sci.* 295, 282–308.

538 Coleman, M.L., Raiswell, R., 1980. Carbon , oxygen and sulphur isotope variations in concretions
539 from the Upper Lias of N . E . England. *Geochim. Cosmochim. Acta* 45, 329–340.

540 Curtis, C., Building, B., Sheffield, S., 1987. Mineralogical consequences of organic matter degradation
541 in sediments : inorganic / organic, in: Leggett, J.K., Zuffa, G.G. (Eds.), *Marine Clastic*
542 *Sedimentology*. pp. 108–123.

543 Dale, A., John, C.M., Mozley, P.S., Smalley, P.C., Muggeridge, A.H., 2014. Time-capsule concretions:
544 Unlocking burial diagenetic processes in the Mancos Shale using carbonate clumped isotopes.
545 *Earth Planet. Sci. Lett.* 394, 30–37. <https://doi.org/10.1016/j.epsl.2014.03.004>

546 De Boever, E., Birgel, D., Thiel, V., Muchez, P., Peckmann, J., Dimitrov, L., Swennen, R., 2009. The
547 formation of giant tubular concretions triggered by anaerobic oxidation of methane as revealed
548 by archaeal molecular fossils (Lower Eocene, Varna, Bulgaria). *Palaeogeogr. Palaeoclimatol.*
549 *Palaeoecol.* 280, 23–36. <https://doi.org/10.1016/j.palaeo.2009.05.010>

550 de Craen, M., Swennen, R., Keppens, E.M., Macaulay, C.I., Kiriakoulakis, K., 1999. Bacterially
551 mediated formation of carbonate concretions in the Oligocene Boom Clay of Northern Belgium.
552 <https://doi.org/10.2110/jsr.69.1098>

553 Dong, J., Zhang, S., Jiang, G., Zhao, Q., Li, H., Shi, X., Liu, J., 2008. Early diagenetic growth of
554 carbonate concretions in the upper Doushantuo Formation in South China and their
555 significance for the assessment of hydrocarbon source rock. *Sci. China Ser. D Earth Sci.* 51,
556 1330–1339. <https://doi.org/10.1007/s11430-008-0107-3>

557 Duan, W.M., Hedrick, D.B., Pye, K., Coleman, M.L., White, D.C., 1996. A preliminary study of the
558 geochemical and microbiological characteristics of modern sedimentary concretions. *Limnol.*
559 *Oceanogr.* 41, 1404–1414. <https://doi.org/10.4319/lo.1996.41.7.1404>

560 Frimmel, A., Oschmann, W., Schwark, L., 2004. Chemostratigraphy of the Posidonia Black Shale, SW
561 Germany I. Influence of sea-level variation on organic facies evolution. *Chem. Geol.* 206, 199–
562 230. <https://doi.org/10.1016/j.chemgeo.2003.12.007>

563 Gómez, J.J., Comas-Rengifo, M.J., Goy, A., 2016. Palaeoclimatic oscillations in the Pliensbachian
564 (Early Jurassic) of the Asturian Basin (Northern Spain). *Clim. Past* 12, 1199–1214.
565 <https://doi.org/10.5194/cp-12-1199-2016>

566 Grice, K., Gibbison, R., Atkinson, J.E., Schwark, L., Eckardt, C.B., Maxwell, J.R., 1996. Maleimides (1H-
567 pyrrole-2,5-diones) as Molecular Indicators of Anoxygenic Photosynthesis in Ancient Water
568 Columns. *Geochim. Cosmochim. Acta* 60, 3913–3924. [https://doi.org/10.1016/0016-](https://doi.org/10.1016/0016-7037(96)00199-8)
569 [7037\(96\)00199-8](https://doi.org/10.1016/0016-7037(96)00199-8)

570 Grice, K., Holman, A.I., Plet, C., Tripp, M., Grice, K., Holman, A.I., Plet, C., Tripp, M., 2019. Fossilised
571 Biomolecules and Biomarkers in Carbonate Concretions from Konservat-Lagerstätten. *Miner.*
572 2019, Vol. 9, Page 158 9, 158. <https://doi.org/10.3390/MIN9030158>

573 Grice, K., Schouten, S., Nissenbaum, A., Charrach, J., Sinninghe Damsté, J.S., 1998. Isotopically heavy
574 carbon in the C21 to C25 regular isoprenoids in halite-rich deposits from the Sdom Formation,
575 Dead Sea Basin, Israel. *Org. Geochem.* 28, 349–359. [https://doi.org/10.1016/S0146-](https://doi.org/10.1016/S0146-6380(98)00006-0)
576 [6380\(98\)00006-0](https://doi.org/10.1016/S0146-6380(98)00006-0)

577 Grice, K., Twitchett, R.J., Alexander, R., Foster, C.B., Looy, C., 2005. A potential biomarker for the
578 Permian–Triassic ecological crisis. *Earth Planet. Sci. Lett.* 236, 315–321.
579 <https://doi.org/10.1016/j.epsl.2005.05.008>

580 Grotheer, H., Le Métayer, P., Piggott, M.J., Lindeboom, E.J., Holman, A.I., Twitchett, R.J., Grice, K.,
581 2017. Occurrence and significance of phytanyl arenes across the Permian-Triassic boundary
582 interval. *Org. Geochem.* 104, 42–52. <https://doi.org/10.1016/j.orggeochem.2016.12.002>

583 Haq, B.U., 2018. Triassic eustatic variations reexamined. *GSA Today* 28, 4–9.

584 <https://doi.org/10.1130/GSATG381A.1>

585 Hendry, J.P., Pearson, M.J., Trewin, N.H., Fallick, A.E., 2006. Jurassic septarian concretions from NW
586 Scotland record interdependent bacterial, physical and chemical processes of marine mudrock
587 diagenesis. *Sedimentology* 53, 537–565. <https://doi.org/10.1111/j.1365-3091.2006.00779.x>

588 Hermoso, M., Minoletti, F., Pellenard, P., 2013. Black shale deposition during Toarcian super-
589 greenhouse driven by sea level. *Clim. Past* 9, 2703–2712. [https://doi.org/10.5194/cp-9-2703-](https://doi.org/10.5194/cp-9-2703-2013)
590 2013

591 Hesselbo, S., Grocke, D., Jenkyns, H.C., Bjerrum, C.J., Farrimond, P., Morgans Bell, H., Green, O.,
592 2000. Massive dissociation of gas hydrate during a Jurassic oceanic anoxic event. *Nature* 406,
593 392–395. <https://doi.org/10.1038/35019044>

594 Hinrichs, K., Boetius, A., 2002. The anaerobic oxidation of methane : new insights in microbial
595 ecology and biogeochemistry, in: Van Weering, T. (Ed.), *Ocean Margin Systems*. Springer, Berlin
596 Heidelberg, pp. 457–477.

597 Holman, A.I., Grice, K., 2018. $\delta^{13}\text{C}$ of aromatic compounds in sediments, oils and atmospheric
598 emissions: A review. *Org. Geochem.* 123, 27–37.
599 <https://doi.org/10.1016/j.orggeochem.2018.06.004>

600 Huggett, J.M., 1994. Diagenesis of Mudrocks and Concretions from the London Clay Formation in the
601 London Basin. *Clay Miner.* 29, 693–707. <https://doi.org/10.1180/claymin.1994.029.4.22>

602 Hussler, G., Connan, J., Albrecht, P., 1984. Novel families of tetra- and hexacyclic aromatic hopanoids
603 predominant in carbonate rocks and crude oils. *Org. Geochem.* 6, 39–49.
604 [https://doi.org/10.1016/0146-6380\(84\)90025-1](https://doi.org/10.1016/0146-6380(84)90025-1)

605 Kemp, D.B., Coe, A.L., Cohen, A.S., Schwark, L., 2005. Astronomical pacing of methane release in the
606 Early Jurassic period. *Nature* 437, 396–399. <https://doi.org/10.1038/nature04037>

607 Killops, S.D., 1991. Novel aromatic hydrocarbons of probable bacterial origin in a Jurassic lacustrine
608 sequence. *Org. Geochem.* 17, 25–36. [https://doi.org/10.1016/0146-6380\(91\)90037-K](https://doi.org/10.1016/0146-6380(91)90037-K)

609 Kiriakoulakis, K., Marshall, J.D., Wolff, G.A., 2000. Biomarkers in a Lower Jurassic concretion from
610 Dorset (UK). *J. Geol. Soc. London.* 157, 207–220. <https://doi.org/10.1144/jgs.157.1.207>

611 Lash, G.G., Blood, D., 2004. Geochemical and textural evidence for early (shallow) diagenetic growth
612 of stratigraphically confined carbonate concretions, Upper Devonian Rhinestreet black shale,
613 western New York. *Chem. Geol.* 206, 407–424. <https://doi.org/10.1016/j.chemgeo.2003.12.017>

614 Lengger, S.K., Melendez, I.M., Summons, R.E., Grice, K., 2017. Mudstones and embedded
615 concretions show differences in lithology-related, but not source-related biomarker
616 distributions. *Org. Geochem.* 113, 67–74. <https://doi.org/10.1016/j.orggeochem.2017.08.003>

617 Lin, Z., Sun, X., Peckmann, J., Lu, Y., Xu, L., Strauss, H., Zhou, H., Gong, J., Lu, H., Teichert, B.M.A.,
618 2016. How sulfate-driven anaerobic oxidation of methane affects the sulfur isotopic
619 composition of pyrite: A SIMS study from the South China Sea. *Chem. Geol.* 440, 26–41.
620 <https://doi.org/10.1016/j.chemgeo.2016.07.007>

621 Long, J.A., Trinajstic, K., 2010. The Late Devonian Gogo Formation Lagerstätte of Western Australia:
622 Exceptional Early Vertebrate Preservation and Diversity. *Annu. Rev. Earth Planet. Sci.* 38, 255–
623 279. <https://doi.org/10.1146/annurev-earth-040809-152416>

624 Marshall, J.D., Pirrie, D., 2013. Carbonate concretions-explained. *Geol. Today* 29, 53–62.
625 <https://doi.org/10.1111/gto.12002>

626 Martill, D.M., 1989. The Medusa effect: instantaneous fossilization. *Geol. Today* 5, 201–205.
627 <https://doi.org/10.1111/j.1365-2451.1989.tb00671.x>

628 Martill, D.M., 1988. Preservation of fish in the Cretaceous Santana Formation of Brazil.
629 *Palaeontology* 31, 1–18.

630 Marynowski, L., Zatoń, M., Simoneit, B.R.T.T., Otto, A., Jedrysek, M., Grelowski, C., Kurkiewics, S.,
631 Jędrysek, M.O., Grelowski, C., Kurkiewicz, S., 2007. Compositions, sources and depositional
632 environments of organic matter from the Middle Jurassic clays of Poland. *Appl. Geochemistry*
633 22, 2456–2485. <https://doi.org/10.1016/j.apgeochem.2007.06.015>

634 McArthur, J.M., Algeo, T.J., van de Schootbrugge, B., Li, Q., Howarth, R., 2008. Basinal restriction,
635 black shales, Re-Os dating, and the Early Toarcian (Jurassic) oceanic anoxic event.
636 *Paleoceanography* 23.

637 Melendez, I., Grice, K., Schwark, L., 2013a. Exceptional preservation of Palaeozoic steroids in a
638 diagenetic continuum. *Sci. Rep.* 3, 2768. <https://doi.org/10.1038/srep02768>

639 Melendez, I., Grice, K., Trinajstić, K., Ladjavardi, M., Greenwood, P., Thompson, K., 2013b.
640 Biomarkers reveal the role of photic zone euxinia in exceptional fossil preservation: An organic
641 geochemical perspective. *Geology* 41, 123–126. <https://doi.org/10.1130/G33492.1>

642 Ogihara, S., 1999. Geochemical characteristics of phosphorite and carbonate nodules from the
643 Miocene Funakawa Formation, western margin of the Yokote Basin, northeast Japan.
644 *Sediment. Geol.* 125, 69–82. [https://doi.org/10.1016/S0037-0738\(98\)00136-5](https://doi.org/10.1016/S0037-0738(98)00136-5)

645 Ogihara, S., Ishiwatari, R., 1998. Unusual distribution of hydrocarbons in a hydrothermally altered
646 phosphorite nodule from Kusu Basin, northern Kyushu, Japan. *Org. Geochem.* 29, 155–161.
647 [https://doi.org/10.1016/S0146-6380\(98\)00052-7](https://doi.org/10.1016/S0146-6380(98)00052-7)

648 Ostroukhov, S.B., Aref'yev, O.A., Zabrodina, M.N., Petrov, A.A., 1983. C12-C30 petroleum
649 alkylbenzenes with regular isoprenane chains. *Pet. Chem. USSR* 23, 217–226.

650 Pearson, M.J., Hendry, J.P., Taylor, C.W., Russell, M.A., 2005. Fatty acids in sparry calcite fracture fills
651 and microsparite cement of septarian diagenetic concretions. *Geochim. Cosmochim. Acta* 69,
652 1773–1786. <https://doi.org/10.1016/j.gca.2004.09.024>

653 Pearson, M.J., Nelson, C.S., 2005. Organic geochemistry and stable isotope composition of New

654 Zealand carbonate concretions and calcite fracture fills. *New Zeal. J. Geol. Geophys.* 48, 395–
655 414. <https://doi.org/10.1080/00288306.2005.9515122>

656 Plet, C., Grice, K., Pagès, A., Ruebsam, W., Coolen, M.J.L., Schwark, L., 2016. Microbially-mediated
657 fossil-bearing carbonate concretions and their significance for palaeoenvironmental
658 reconstructions: A multi-proxy organic and inorganic geochemical appraisal. *Chem. Geol.* 426,
659 95–108. <https://doi.org/10.1016/j.chemgeo.2016.01.026>

660 Plet, C., Grice, K., Pagès, A., Verrall, M., Coolen, M.M.J.L., Ruebsam, W., Rickard, W.D.A., Schwark, L.,
661 2017. Palaeobiology of red and white blood cell-like structures, collagen and cholesterol in an
662 ichthyosaur bone. *Sci. Rep.* 7, 13776. <https://doi.org/10.1038/s41598-017-13873-4>

663 Pye, K., Dickson, J.A.D., Schiavon, N., Coleman, M.L., Cox, M., 1990. Formation of siderite-Mg-calcite-
664 iron sulphide concretions in intertidal marsh and sandflat sediments, north Norfolk, England.
665 *Sedimentology* 37, 325–343. <https://doi.org/10.1111/j.1365-3091.1990.tb00962.x>

666 Raiswell, R., Fisher, Q.J., 2000. Mudrock-hosted carbonate concretions: a review of growth
667 mechanisms and their influence on chemical and isotopic composition. *J. Geol. Soc. London.*
668 157, 239–251. <https://doi.org/10.1144/jgs.157.1.239>

669 Reitner, J., Peckmann, J., Blumenberg, M., Michaelis, W., Reimer, A., Thiel, V., 2005. Concretionary
670 methane-seep carbonates and associated microbial communities in Black Sea sediments.
671 *Palaeogeogr. Palaeoclimatol. Palaeoecol.* 227, 18–30.
672 <https://doi.org/10.1016/j.palaeo.2005.04.033>

673 Riding, R., 2000. Microbial carbonates: the geological record of calcified bacterial-algal mats and
674 biofilms. *Sedimentology* 47, 179–214.

675 Rodrigues, B., Silva, R.L., Reolid, M., Filho, J.G.M., Duarte, L.V., 2019. Sedimentary organic matter
676 and $\delta^{13}\text{C}$ Kerogen variation on the southern Iberian palaeomargin (Betic Cordillera, SE Spain)
677 during the latest Pliensbachian–Early Toarcian. *Palaeogeogr. Palaeoclimatol. Palaeoecol.* 534.

678 Röhl, H.-J., Schmid-Röhl, A., 2005. Lower Toarcian (Upper Liassic) Black Shales of the Central
679 European Epicontinental Basin: A Sequence Stratigraphic Case Study from the Sw German
680 Posidonia Shale. *Depos. Org. Sediments Model.* 165–189.
681 <https://doi.org/10.2110/pec.05.82.0165>

682 Röhl, H., Schmid-Röhl, A., Oschmann, W., Frimmel, A., Schwark, L., 2001. The Posidonia Shale (Lower
683 Toarcian) of SW-Germany : an oxygen-depleted ecosystem controlled by sea level and
684 palaeoclimate. *Palaeogeogr. Palaeoclimatol. Palaeoecol.* 165, 27–52.

685 Ruebsam, W., Mayer, B., Schwark, L., 2019. Cryosphere carbon dynamics control early Toarcian
686 global warming and sea level evolution. *Glob. Planet. Change* 172, 440–453.
687 <https://doi.org/10.1016/j.gloplacha.2018.11.003>

688 Ruebsam, W., Müller, T., Kovács, J., Pálffy, J., Schwark, L., 2018. Environmental response to the early
689 Toarcian carbon cycle and climate perturbations in the northeastern part of the West-Tethyl
690 shelf. *Gondwana Res.* 59, 144–158.

691 Schmid-Röhl, A., Röhl, H., Oschmann, W., Frimmel, A., 2002. Palaeoenvironmental reconstruction of
692 Lower Toarcian epicontinental black shales (Posidonia Shale , SW Germany): global versus
693 regional control. *Geobios* 35, 13–20.

694 Schouten, S., Van Kaam-Peters, H.M.E., Rijpstra, W.I.C., Schoell, M., Sinninghe Damste, J.S., 2000.
695 Effects of an oceanic anoxic event on the stable carbon isotopic composition of early Toarcian
696 carbon. *Am. J. Sci.* 300, 1–22.

697 Schwark, L., Frimmel, A., 2004. Chemostratigraphy of the Posidonia Black Shale, SW-Germany II.
698 Assessment of extent and persistence of photic-zone anoxia using aryl isoprenoid distributions.
699 *Chem. Geol.* 206, 231–248. <https://doi.org/10.1016/j.chemgeo.2003.12.008>

700 Scotchman, I.C., 1991. The geochemistry of concretions from the Kimmeridge Clay Formation of
701 southern and eastern England. *Sedimentology* 38, 79–106. <https://doi.org/10.1111/j.1365->

702 3091.1991.tb01856.x

703 Sinninghe Damsté, J.P., Kock-Van Dalen, A.C., De Leeuw, J.W., Schenck, P.A., Brassell, S.C., 1987. The
704 identification of mono-, di- and trimethyl 2-methyl-2-(4,8,12-trimethyltridecyl)chromans and
705 their occurrence in the geosphere. *Geochim. Cosmochim. Acta* 5, 2393–2400.

706 Sinninghe Damsté, J.S., De Leeuw, J.W., Schenck, P. a, 1988a. Organically-Bound Sulphur in the
707 Geosphere: a Molecular Approach. Tech. Univ. Delft PhD., 287.

708 Sinninghe Damsté, J.S., Keely, B.J., Betts, S.E., Baas, M., Maxwell, J.R., De Leeuw, J.W., 1993.
709 Variations in abundances and distributions of isoprenoid chromans and long-chain
710 alkylbenzenes in sediments of the Mulhouse Basin : a molecular sedimentary record of
711 palaeosalinity *. *Org. Geochem.* 20, 1201–1215.

712 Sinninghe Damsté, J.S., Kock-van Dalen, A.C., de Leeuw, J.W., 1988b. Identification of long-chain
713 isoprenoid alkylbenzenes in sediments and crude oils. *Geochim. Cosmochim. Acta* 52, 2671–
714 2677. [https://doi.org/10.1016/0016-7037\(88\)90035-X](https://doi.org/10.1016/0016-7037(88)90035-X)

715 Sinninghe Damsté, J.S., Köster, J., Baas, M., Ossebaar, J., Dekker, M., Pool, W., Geenevasen, J.A.J.,
716 1999. A sedimentary tetrahydrophenanthrene derivative of tetrahymanol. *Tetrahedron Lett.*
717 40, 3949–3952. [https://doi.org/10.1016/S0040-4039\(99\)00618-8](https://doi.org/10.1016/S0040-4039(99)00618-8)

718 Thiel, V., Hoppert, M., 2018. Fatty acids and other biomarkers in two Early Jurassic concretions and
719 their immediate host rocks (Lias δ Buttenheim clay pit, Bavaria, Germany). *Org. Geochem.* 120,
720 42–55. <https://doi.org/10.1016/j.orggeochem.2018.02.010>

721 Trolio, R., Grice, K., Fisher, S.J., Alexander, R., Kagi, R.I., 1999. Alkylbiphenyls and
722 alkylidiphenylmethanes as indicators of petroleum biodegradation. *Org. Geochem.* 30, 1241–
723 1253. [https://doi.org/10.1016/S0146-6380\(99\)00099-6](https://doi.org/10.1016/S0146-6380(99)00099-6)

724 Tulipani, S., Grice, K., Greenwood, P.F., Haines, P.W., Sauer, P.E., Schimmelmann, A., Summons, R.E.,
725 Foster, C.B., Böttcher, M.E., Playton, T., Schwark, L., 2015. Changes of palaeoenvironmental

726 conditions recorded in Late Devonian reef systems from the Canning Basin, Western Australia:
727 A biomarker and stable isotope approach. *Gondwana Res.* 28, 1500–1515.
728 <https://doi.org/10.1016/j.gr.2014.10.003>

729 Werne, J.P., Lyons, T.W., Hollander, D.J., Formolo, M.J., Sinninghe Damsté, J.S., 2003. Reduced sulfur
730 in euxinic sediments of the Cariaco Basin: Sulfur isotope constraints on organic sulfur
731 formation. *Chem. Geol.* 195, 159–179. [https://doi.org/10.1016/S0009-2541\(02\)00393-5](https://doi.org/10.1016/S0009-2541(02)00393-5)

732 Wilkin, R.T., Arthur, M.A., 2001. Variations in pyrite texture , sulfur isotope composition , and iron
733 systematics in the Black Sea : Evidence for Late Pleistocene to Holocene ... *Geochemica*
734 *Cosmochim. Acta* 65, 1399–1416. [https://doi.org/10.1016/S0016-7037\(01\)00552-X](https://doi.org/10.1016/S0016-7037(01)00552-X)

735 Wilkin, R.T., Barnes, H.L., 1997. Formation processes of framboidal pyrite. *Geochemica Cosmochim.*
736 *Acta* 61, 323–339.

737 Williams, J.A., Dolcater, D.L., Torkelson, B.E., Winters, J.C., 1988. Anomalous concentrations of
738 specific alkylaromatic and alkylcycloparaffin components in West Texas and Michigan crude
739 oils. *Org. Geochem.* 13, 47–60. [https://doi.org/10.1016/0146-6380\(88\)90024-1](https://doi.org/10.1016/0146-6380(88)90024-1)

740 Williams, M., Benton, M.J., Ross, A., 2015. The Strawberry Bank Lagerstätte reveals insights into
741 Early Jurassic life. *J. Geol. Soc. London.* 2014–144. <https://doi.org/10.1144/jgs2014-144>

742 Wolff, G.A., Rukin, N., Marshall, J.D., 1992. Geochemistry of an early diagenetic concretion from the
743 Birchi Bed (L. Lias, W. Dorset, U.K.). *Org. Geochem.* 19, 431–444. [https://doi.org/10.1016/0146-](https://doi.org/10.1016/0146-6380(92)90010-U)
744 [6380\(92\)90010-U](https://doi.org/10.1016/0146-6380(92)90010-U)

745 Woo, K.S., Khim, B.K., 2006. Stable oxygen and carbon isotopes of carbonate concretions of the
746 Miocene Yeonil Group in the Pohang Basin, Korea: Types of concretions and formation
747 condition. *Sediment. Geol.* 183, 15–30. <https://doi.org/10.1016/j.sedgeo.2005.09.005>

748 Yoshida, H., Asahara, Y., Yamamoto, K., Katsuta, N., Minami, M., Metcalfe, R., 2019. $^{87}\text{Sr}/^{86}\text{Sr}$ age
749 determination by rapidly formed spherical carbonate concretions. *Sci. Rep.* 9, 1003.

750 <https://doi.org/10.1038/s41598-019-38593-9>

751 Yoshida, H., Ujihara, A., Minami, M., Asahara, Y., Katsuta, N., Yamamoto, K., Sirono, S., Maruyama, I.,
752 Nishimoto, S., 2015. Early post-mortem formation of carbonate concretions around tusk-shells
753 over week-month timescales. *Sci. Rep.* 1–7. <https://doi.org/10.1038/srep14123>

754 Yoshida, H., Yamamoto, K., Minami, M., Katsuta, N., Sin-Ichi, S., Metcalfe, R., 2018. Generalized
755 conditions of spherical carbonate concretion formation around decaying organic matter in
756 early diagenesis. *Sci. Rep.* 8, 1–10. <https://doi.org/10.1038/s41598-018-24205-5>

757 Zatoń, M., Marynowski, L., 2004. Konzentrat-Lagerstätte-type carbonate concretions from the
758 uppermost Bajocian (Middle Jurassic) of the Czêstochowa area , South-Cental Poland. *Geol. Q.*
759 48, 339–350.

760 Zhang, S., Huang, H., Su, J., Liu, M., Zhang, H., 2014. Organic Geochemistry Geochemistry of
761 alkylbenzenes in the Paleozoic oils from the Tarim. *Org. Geochem.* 77, 126–139.
762 <https://doi.org/10.1016/j.orggeochem.2014.10.003>

763 Ziegler, P.A., 1990. Geological Atlas of Western and Central Europe. Shell Internationale Petroleum
764 Mij. B. V. and Geological Society, London.

765

766

767 **FIGURE CAPTIONS**

768 **Figure 1.** Concretions A and B showing the positions and labelling of subsamples investigated.
769 Subsample 1 being the most internal and subsample 3 corresponding to the concretion rim.

770 **Figure 2.** GC-MS total ion chromatogram (TIC) of the host sediment compared to body and rim
771 samples of concretion A (left) and B (right). Vertical exaggeration was applied on the chromatograms
772 to reveal the compounds of interest. DBT: dibenzothiophene; IS: internal standard; mDBT:
773 methyldibenzothiophene; PT: phytanyl toluene; MTTC: methyltrimethyltridecylchromans. Peaks
774 labelled I and II are tentatively identified as 1,1,7,8-tetramethyl-1,2,3,4-tetrahydrophenanthrene and
775 a C₃ alkylphenanthrene.

776 **Figure 3.** Relative distribution of MTTCs, MPs + MDBTs, and C₂₆-C₂₈ TAS within all samples studied.
777 Most concretion samples show a higher TAS proportion than the host sediment (PS).

778 **Figure 4.** Both concretions showed similar extracted ion chromatograms, here represented by the
779 chromatograms from concretion B. GC-MS and GC×GC-ToF-MS chromatograms of extracted ions
780 m/z 92 for alkylated benzenes (AlkB) and phytanyl benzene (PB) on the left and m/z 106 for alkylated
781 toluene (AlkT) and phytanyl toluene (PT) on the right. Comparison of the distribution from the host
782 sediment and concretion B (representative of both concretion). Vertical exaggeration has been
783 reported for the GC-MS data in order to facilitate the comparison.

784 **Figure 5.** Correlation between phytanyl and n-alkylated arenes in the sample set.

785 TABLES AND TABLE CAPTIONS

786

787 *Table 1. Compilation of publications reporting lipid biomarkers in carbonate concretions and main findings based on biomarker analyses.*

Age	Location	Reported mineralogy	lipids investigated	Main highlights from lipids & biomarkers	reference
Lower Lias	UK	calcite, (Fe)dolomite	aliphatic hydrocarbons, fatty acids	Mineralogical zonation derived from different microbial communities. Microbial activity involved: sulfate reduction, methanogenesis, iron and manganese-reducing activity	(Wolff et al., 1992)
Present	UK	Calcite, siderite, iron monosulfide	polar lipid fatty acids	Two sulfate reducing bacteria genera: <i>Desulfovibrio</i> sp. > <i>Desulfobacter</i> sp.	(Coleman, 1993)
Present	Middle Valley, Juan de Fuca Ridge	calcite-cemented soft mud, silt and pyrite	hydrocarbons	Biomarkers reflect high thermal maturity providing information on the geological history	(Boni et al., 1994)
Present	UK	siderite, calcite, fluorapatite, rhodochrosite, quartz, clay minerals, pyrite	Fatty acids, phospholipid fatty acids (PLFA)	Variations of lipid biomarker distributions within a single concretion, between individual concretions and between concretions and host sediments Great diversity of sulfate-reducing bacterial biomarker Biomarker for <i>Desulfovibrio</i> sp capable of iron-reduction	(Duan et al., 1996)
Pleistocene	Japan	carbonate fluorapatite	aliphatic hydrocarbons and fatty acids	Non-altered phosphorite nodule: high hydrocarbon maturity Altered phosphorite nodule: hydrocarbons derived from microbial activity under hydrothermal condition.	(Ogihara and Ishiwatari, 1998)
Miocene	Japan	calcite, phosphorite, dolomite	aliphatic hydrocarbons, ketones	Low maturity and high hopanoid content. P concentration and apatite precipitation mediated by bacteria in sulfate reduction zone.	(Ogihara, 1999)

Oligocene	Belgium	calcite with framboidal pyrite +detrital minerals in minor amount	aliphatic hydrocarbons and fatty acids	Large terrigenous input and low algal steroidal markers Abundant markers of sulfate-reducing bacteria in the concretion Presence of methanogenic archaeal markers in the concretion.	(de Craen et al., 1999)
Lower Lias	UK	calcite, dolomite	aliphatic hydrocarbons and fatty acids	Biomarkers indicative of sulfate-reducing bacteria in calcite core	(Kiriakoulakis et al., 2000)
Middle Jurassic	Poland		hydrocarbons, fatty acids	Thermally immature OM Predominance of terrestrial biomarkers in host sediment and concretions Diasterene > sterenes> steranes suggest early and shallow formation of carbonate concretions No evidence for water column stratification and anoxia	(Zatoń and Marynowski, 2004)
Late Jurassic	UK	calcite	fatty acids	Different fatty acids distribution between calcite septaria and concretion body Differences attributed to the low aqueous solubility of long chain fatty acids	(Pearson et al., 2005)
Jurassic, Cretaceous, Paleocene, Eocene, Miocene	New Zealand, UK	calcite, siderite, Fe-dolomite	aliphatic hydrocarbons, fatty acids	Concretion septaria: the fatty acids incorporated into septarian calcite during crystal formation Concretions matrix: fatty acids are kerogen derived Input from terrestrial vegetation Strong maturity differences between cracks and concretions	(Pearson and Nelson, 2005)
Present	Black Sea	calcite	Aliphatic hydrocarbons, alcohols	Combined DNA and biomarker analyses on microbial mats and carbonate at methane seep Evidence of archaea and sulfate reducing bacteria, algae and higher plant biomarkers Confirmation of pivotal role for archaea and sulfate-reducing bacteria during carbonate concretions formation in methane seep environments	Reitner 2005
Middle Jurassic	Poland	Siderite, rhodochrosite, calcite, dolomite	hydrocarbons, fatty acids	Comparison of biomarker from host sediment and concretion: similar hydrocarbon distribution but different fatty acid distribution Unsaturated fatty acids higher in concretions than host sediment No sulfate-reducing bacterial marker detected	(Marynowski et al., 2007)
Lower Eocene	Bulgaria	Calcite with detrital grains (quartz, feldspar)	alcohols, Fatty acids	Release of carbonate-bound and ester bound biomarkers Abundant archaeal biomarkers, bacterial markers and eukaryotic markers	(De Boever et al., 2009)

Devonian	Australia	Calcite	aliphatic and aromatic hydrocarbons	¹³ C-depleted <i>n</i> -alkane distribution attributed to sulfate reducing bacteria High cholestane with distinct ¹³ C signature attributed to fossil crustacean Aromatic hydrocarbon showed evidence of photic zone euxinia during concretion formation	(Melendez et al., 2013b)
Devonian	Australia	Calcite	steroids	Fossil preserved in concretion revealed presence of a steroid continuum (from sterols to triaromatic steroids) Oldest intact sterols reported in the rock record	(Melendez et al., 2013a)
Upper Miocene	Austria	Siderite, calcite	hydrocarbons, fatty acids	Low overall content of bacterial biomarkers	(Baumann et al., 2016)
Toarcian	Germany	Calcite, pyrite	aliphatic hydrocarbons, aryl isoprenoids	Similar biomarker distribution between two concretions and their host sediment indicate biomarker signature inherited from host sediment ¹³ C depletion of <i>n</i> -alkanes in the concretions compared to host sediment related to sulfate reducing bacterial activity	(Plet et al., 2016)
Toarcian	Germany	Calcite, pyrite	steroids	Preservation of intact sterols in the fossil vertebra embedded in a concretion Sterols $\delta^{13}\text{C}$ composition revealed two sources of sterols: C ₂₇ sterol largely derived from the ichthyosaur diet, C ₂₉ sterol derived from primary activity in the water column	(Plet et al., 2017)
Devonian	Australia	Calcite cement with pyrite and detrital grain	total lipid extract (focus on aliphatic hydrocarbons)	Aliphatic hydrocarbons of concretions similar to host sediment: aliphatic distribution inherited during concretion formation Variations exist in biomarker indices related to lithology (carbonate vs. mudstone)	(Lengger et al., 2017)
Toarcian	Germany	siderite, calcite, fluorapatite, rhodochrosite, quartz, clay minerals, pyrite	fatty acids, hydrocarbons	Evidence of enhanced preservation or selective accumulation mechanism of fatty acids and diacids in the concretions compared to the host sediment	(Thiel and Hoppert, 2018)

789 Table 2. Proportions of TOC, CaCO₃, pyrite and siliciclastic component of each samples (in %). $\delta^{34}\text{S}_{\text{bulk}}$ for each sample. * is
 790 an average of two PS samples. † values published in Plet et al., 2016.

	HI † (mg HC / gTOC)	TOC (wt%)	CaCO₃ † (wt%)	Pyrite (wt%)	Siliciclastic (wt%)	$\delta^{34}\text{S}_{\text{bulk}}$	$\delta^{13}\text{C}_{\text{carbonate}}$ †
PS	820	9.4	40	7	43.4	-21.9*	-1.8
A1	740	1.0	95	1	3.1	--17.0	-14.5
A2	750	1.0	95	1	3.1	--15.5	-14.4
A3	580	1.0	83	13	2.8	-8.4	-12.6
B1	700	0.9	96	1	2.3	-11.7	-10.2
B2	720	0.8	95	1	3.3	-15.5	-14.2
B3	590	2.1	70	22	6.5	-8	-8.3

791

792 Table 3. Normalisation of compounds and groups of compounds to the sum of C₂₆-C₂₈ TAS. *indicates ratios determined
 793 based on GC×GC-ToF-MS analyses. AlkBr: alkylbenzene ratio; PBr: phytanyl benzene/C₂₆-C₂₈ TAS; AlkTr: alkyltoluene
 794 ratio; PTr: phytanyl toluene/C₂₆-C₂₈ TAS; C₁₈ BrTr= C₁₈ BrT*1000/sum C₂₆-C₂₈ TAS; BrTr= sum C₁₆-C₂₆ BrT*1000/ sum C₂₆-C₂₈
 795 TAS; DBTr: DBT/C₂₆-C₂₈; MDBTr: sum MDBT/C₂₆-C₂₈ TAS; DMDBTr: sum DMDBT/sum C₂₆-C₂₈ TAS, BNTr: sum BNT/C₂₆-C₂₈
 796 TAS; AlkNr: sum alkyl naphthalene/C₂₆-C₂₈ TAS; C₂₉DESHr: C₂₉DESH*1000/C₂₆-C₂₈TAS; BHR: sum C₃₂-C₃₃ benzohopanes/C₂₆-
 797 C₂₈ TAS.

	Host sediment	Concretion A			Concretion B		
		A1	A2	A3	B1	B2	B3
ratios	PS						
AlkBr*	0.06	0.90	0.17	0.88	1.75	1.10	1.02
PBr *	<0.01	0.01	<0.01	0.04	0.04	0.03	0.02
AlkTr*	0.31	2.53	1.33	1.95	3.24	2.87	2.04
BrTr*	16	259	58	227	356	265	171
PTr*	0.06	0.53	0.26	0.81	0.77	0.73	0.69
DBTr	0.16	0.15	0.10	0.10	0.21	0.13	0.11
MDBTr	0.47	0.38	0.26	0.22	0.61	0.42	0.31
DMDBTr	0.41	0.32	0.20	0.29	0.56	0.41	0.29
BNTr	0.09	0.06	0.04	0.06	0.12	0.09	0.06
AlkNr	3.77	6.69	4.48	4.87	9.76	6.82	4.83
C ₂₉ DESHr*	1.8	3.77	3.78	3.72	4.31	4.71	5.99
BHR*	202	116	n.d.	202	178	141	248

798